Chapter 4

Quasistatic and Dynamic Responses of HCNT Foams[3]

We describe the quasistatic and dynamic response of helical carbon nanotube (HCNT) foams in compression, and compare their mechanical properties to those reported earlier for vertically aligned carbon nanotube (VACNT) foams. Similar to VACNT foams, HCNT foams exhibit preconditioning effects in response to cyclic loading; however, their fundamental deformation mechanisms are significantly different from those of VACNT foams. HCNT foams exhibit strain localization and collective structural buckling, nucleating at different points throughout their thickness, and HCNT micro-bundles often undergo brittle fracture. Regardless of this microstructural damage, bulk HCNT foams exhibit super-compressibility, on par with VACNTs, and recover more than 90% of large compressive strains (up to 80%). When subjected to striker impacts, HCNT foams mitigate impact forces more effectively than VACNT foams—a desirable characteristic for protective applications.

4.1 Introduction

Helical carbon nanotubes (HCNTs) have been synthesized as individual fibers [155], self-assembled ropes [156], or in macroscopic arrays [52,157]. Small-scale HCNT fibers have been fabricated for a variety of applications such as nano-electronics and nano-mechanical systems [158], self-sensing mechanical resonators [159], reinforcement in epoxy based composites [160,161], and energy applications including fuel cells, hydrogen storage and super-capacitors [162,163]. Macroscopic arrays of HCNTs have

[3] This chapter represents a collaboration work with M. Karakaya, E. R. Meshot, A. Fischer, R. Podila and A. M. Rao. MK synthesized samples. RT performed mechanical characterization and analyzed the data. ERM conducted the synchrotron x-ray scattering experiments. RT, AF and MK performed electron microscope characterizations. RT wrote the manuscript with the support of others. We acknowledge ScopeM of ETH Zurich for TEM.

been synthesized for flat panel field emission display [164], electromagnetic shielding [165], and energy dissipative cushioning and packaging [53]. Unlike straight vertically aligned carbon nanotube (VACNT) arrays [37,166], studies on the mechanical response of bulk HCNT foams are sparse in literature [53,77,160,161].

Bulk HCNT foams, similar to VACNT foams, derive their unique mechanical properties from their hierarchically organized microstructures characterized by aligned and entangled helical coils of multi-walled CNTs (Figures 4.1 (a), (b)). The carbon nanocoils act like elastic springs, with their deformation behavior governed by geometric nonlinearity [167]. The spring constant of a helical coil is proportional to the quartic power of the diameter of the coiled wire (CNT diameter), and inversely proportional to the cubic power of the radius of the coil [167]. Such geometric nonlinearity in the deformation of the individual nanocoils leads to an interesting collective mechanical response in the HCNT foams. For example, the contact interaction of a spherical indenter with HCNT foams is highly nonlinear and non-Hertzian, and different from the contact interaction of a spherical indenter with VACNT foams [53]. This highly nonlinear collective response is attributed primarily to the unusual entanglement between neighboring coils and to the collective bending behavior of the coil tips when impacted by a spherical indenter [54]. The HCNT foams have been shown to mitigate low velocity (0.2 ms^{-1}) impact forces efficiently and fully recover deformation of the order ~5 μm (5% strain) [53]. However, their fundamental deformation mechanisms at large strains and different strain-rates have not been studied yet. Below, we present a comprehensive study of the mechanical response of HCNT foams in both quasistatic and dynamic loading regimes with structural characterizations. We performed morphological characterization using synchrotron x-ray scattering and correlated the structural characteristics with the observed fundamental deformation mechanisms under compressive loading. We used *in-situ* high-speed microscopy, scanning electron microscopy (SEM), and transmission electron microscopy (TEM) to elucidate the deformation mechanisms that govern the bulk mechanical behavior.

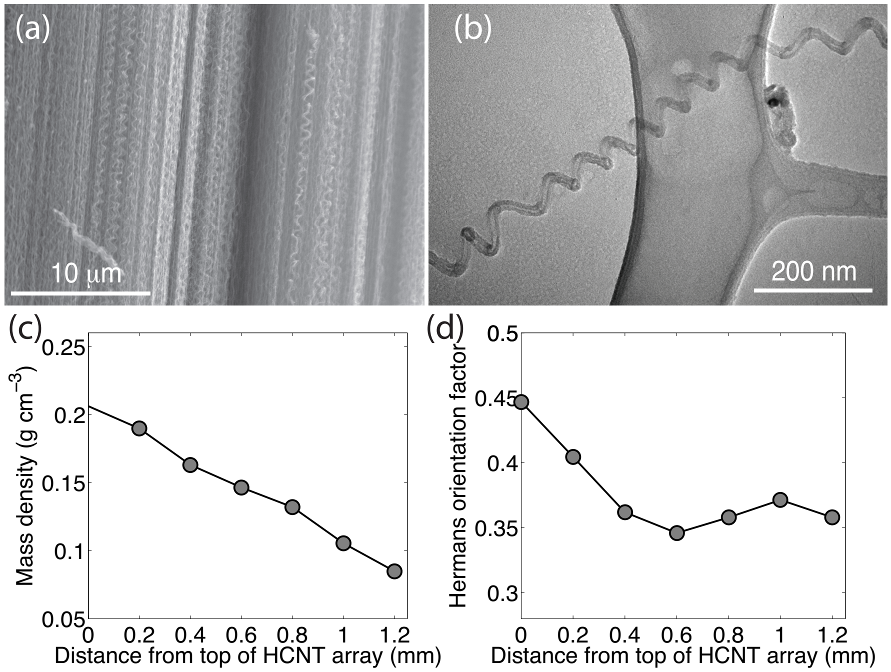

Figure 4.1. Hierarchical morphology of HCNT foams: **(a)** SEM image of vertically aligned bundles of entangled HCNTs, **(b)** TEM image of an individual HCNT, **(c)** mass density gradient along the height of the HCNT foam sample, and **(d)** alignment of the HCNTs within the HCNT foam along the height of the sample.

4.2 Experimental methods

HCNT foams were synthesized using a two-stage thermal chemical vapor deposition (CVD) process as described in the Section 2.1.3. The resultant HCNT foams were ~ 1 mm in heights and had an average density of ~ 0.17 g cm^{-3}. As these samples couldn't be extracted from the substrate as standalone HCNT foams, they were characterized for mechanical properties, whilst still attached to the growth substrates.

We performed synchrotron X-ray scattering and mass attenuation measurements to nondestructively quantify the density and alignment within HCNT foams. Full descriptions on the experimental methods and the analysis are provided in Section 2.2.

The quasistatic compression tests were performed on an *Instron ElectroPulse E3000* testing system as described in Section 2.3. All the quasistatic experiments were performed at 0.01 s^{-1} strain rate. The dynamic experiments were performed on the impact testing setup described in Section 2.4.

4.3 Results and discussions

4.3.1 Morphological characteristics of HCNT foams

SEM and TEM studies were performed to explore the structure and morphology of the as-grown and deformed HCNT foam samples. SEM images of the HCNT foam microstructure reveal the uniformity of the coiling and pitch (Figure 4.1 (a)) of HCNTs present in the array. The thickness of the HCNT foams is ~1 mm and the dominant HCNT diameter and pitch are around 25±5 nm and 50nm, respectively.

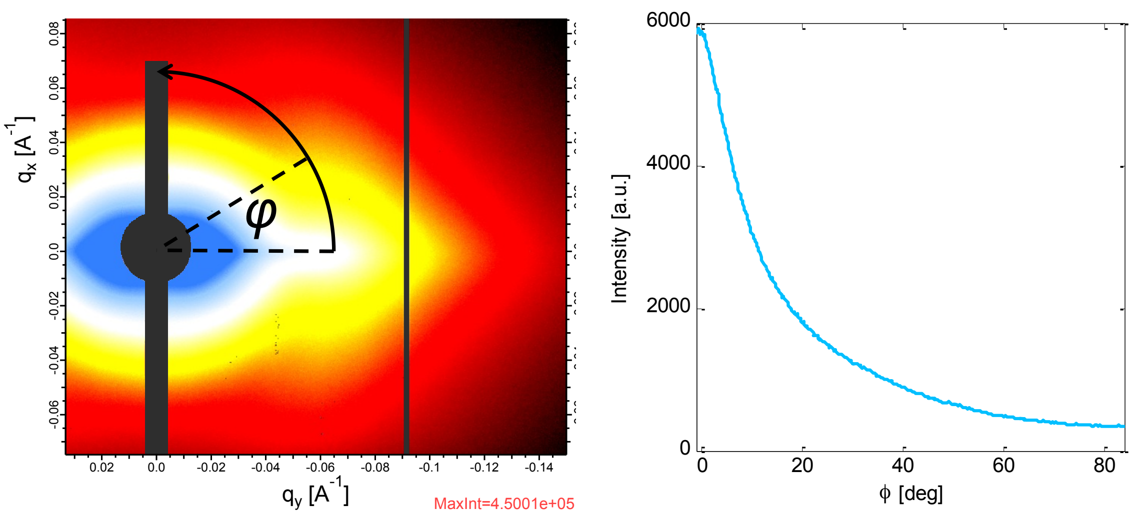

Figure 4.2. A representative small angle x-ray scattering (SAXS) image of an HCNT foam sample. Schematic illustration demonstrates the azimuthal integration we perform on SAXS images to extract the Herman's orientation factor. The annulus of the azimuthal scan about φ is defined by ±5 pixels from the CNT form factor scattering peak located near q = 0.05-0.07 $Å^{-1}$. We only use one half of the SAXS image because HCNT alignment is isotropic in the plane of the catalyst substrate (Si), so the SAXS pattern is vertically symmetric.

The mass density characterized by the synchrotron x-ray scattering and mass attenuation was found to decrease linearly with the height of the HCNT foam, from the top to the bottom (adjacent to substrate), and the average density was 0.15 g cm^{-3} with 59% variation along the height (Figure 4.1(c)). The CNT alignment was quantified from the anisotropy of the SAXS patterns using Herman's orientation factor, f [104,168] (Figure 4.2 shows a representative small angle x-ray scattering (SAXS) image of an HCNT foam sample and the intensity variation with the azimuthal angle). We found that the alignment decreased from the top to the bottom of the sample with the bulk sample having an average alignment of 0.38 (Figure 4.1 (d)). Here, f equals 1 for perfectly aligned CNTs and 0 for random order (no alignment). The low-alignment of the sample is attributed to the coiled nature of the fibers within the HCNT foam.

4.3.2 Quasistatic response of HCNT foams

HCNT foams, when subjected to quasistatic compressive loading-unloading cycles exhibit a nonlinear stress-strain response with a hysteresis loop (Figure 4.3 (a)), similar to other foam materials [147] and to VACNT foams [37]. When an HCNT foam is compressed, the stress rises nonlinearly with strain up to a peak stress, and then falls rapidly along a different path during unloading resulting in a hysteresis. Through hysteresis, the foam dissipates energy but has the ability to recover large compressive strains up to 80%. When the same HCNT foam is compressed again, the loading path differs from the previous loading cycle, exhibiting a preconditioning effect (Figure 4.3 (a)). This effect is pronounced in the first three cycles but the response stabilizes for consecutive cycles beyond the third cycle. A similar preconditioning effect was also reported in compressive studies of VACNT foams and was attributed to microstructural rearrangements of the CNTs during the loading-unloading cycles [37,38]. In the case of HCNT foams, in addition to the microstructural rearrangements, we also observed permanent microstructural damage and brittle fracture of HCNT bundles in the deformed region (Figure 4.3 (f)). The peak stress (Figure 4.3 (b)), the unloading modulus (Figure 4.3 (c)) and the hysteretic energy dissipation (Figure 4.3 (d)) also decrease rapidly within the first three cycles and remain nearly constant for the later cycles, implying that the mechanical properties of HCNT foams are loading-history dependent. The compressive strength (peak stress at 80% strain) of the HCNT foams (22.2±1.4 MPa) and the hysteretic energy dissipation (3.38±0.32 MJ m^{-3}) are comparable to that of the VACNT foams with similar densities [42].

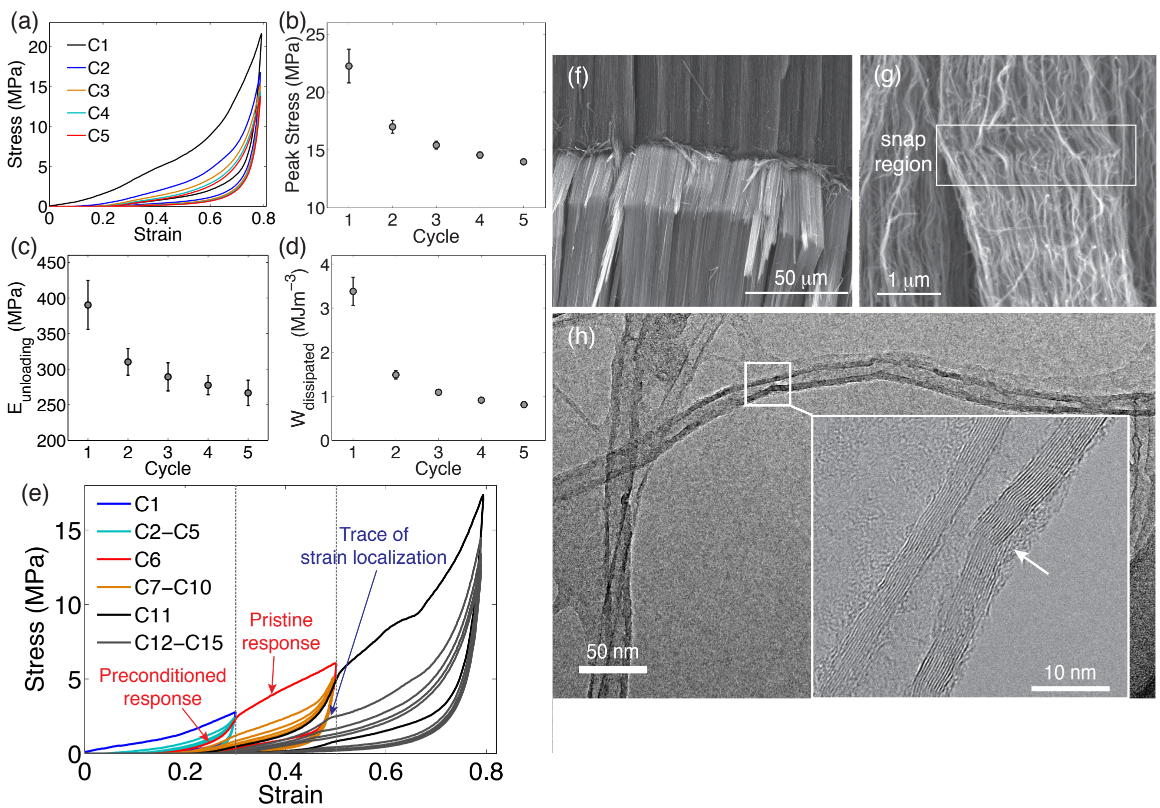

Figure 4.3. (a) Stress strain response of a HCNT foam under quasistatic compression cycles. Variation of **(b)** the peak stress, **(c)** the unloading modulus, and **(d)** the hysteretic energy dissipation with consecutive compression cycles; error bars represent the standard deviation of three samples measured. **(e)** Strain localization and loading history dependent response of an HCNT foam. C1-C5, C6-C10 and C11-C15 correspond to compression cycles with 0.3, 0.5, and 0.8 maximum strains, respectively. **(f-g)** SEM images showing microstructural deformation mechanisms under compression: **(f)** collective structural buckling of the HCNTs exhibiting brittleness in the response, **(g)** snap region of a bundle showing that the deformation is extending to several pitches of the individual HCNTs, which changes their pristine configuration. **(h)** TEM images taken at turning points of pristine individual HCNTs revealing defective/broken walls at the

turning points of the coils.

When an HCNT foam that was subjected to repeated cyclic loading at a moderate strain was compressed beyond the previous maximum strain (30 %), the loading path changed from the preconditioned path to the pristine sample's loading path (Figure 4.3 (e)). This change from preconditioned to pristine response suggests that the strain in the sample is localized and the deformation is not uniform. These regions of strain localization (occurring during the first cycle) are also identifiable in the consecutive cycles (second and later cycles), as indicated on Figure 4.3 (e). This kind of strain localization was also observed for VACNT foams, where the vertically aligned bundles of CNTs undergo a well-defined sequential periodic buckling that is governed by the samples' intrinsic density gradient [37,62,123,145]. However, the strain localization in HCNT foams is surprising, since previous studies suggested primarily a spring-like bulk compressive behavior [53,167]. We correlate this response to the HCNT foam's microstructure, consisting of long entangled HCNTs with length (l ~1 mm), three orders of magnitude higher than the coil diameter (d_{coil} ~450 nm) [165]. Due to (i) the very high aspect ratio (l/d_{coil} ~2000), (ii) entanglement with neighboring coils, and (iii) the vertical alignment of HCNT bundles, the deformation is localized rather than the whole HCNT foam undergoing a uniform deformation. *In-situ* microscopy and SEM characterization of a HCNT foam under compression revealed that the strain initially localizes in the sample's low-density region, near the substrate. After a critical strain of ~10%, localization begins to appear in different regions of the sample's thickness. Several consecutive structural buckles with observable brittleness follow the initial deformation (Figure 4.3 (f)). An SEM image sequence showing the deformation mechanisms during a quasistatic compression cycle is provided in Figure 4.4. The SEM images also reveal the presence of several permanent microstructural deformations and HCNT bundles that underwent brittle fracturing during loading. TEM analysis of pristine (as-grown) HCNTs show that the as-grown nanocoils have numerous structural defects: the multiwalled HCNTs have highly deformed or defective walls at the coils' turning points (indicated by arrow) in Figure 4.3 (h). The presence of a large number of such nanoscale defects present in the pristine samples may have led to the fracture of the bundles when compressed. The bulk samples, however, show significant recovery upon unloading, regardless of the microstructural damages. This suggests that interactions between HCNT bundles at the mesoscale play a dominant role in the bulk response of foams, over the nanoscale permanent damage observed in the individual coils.

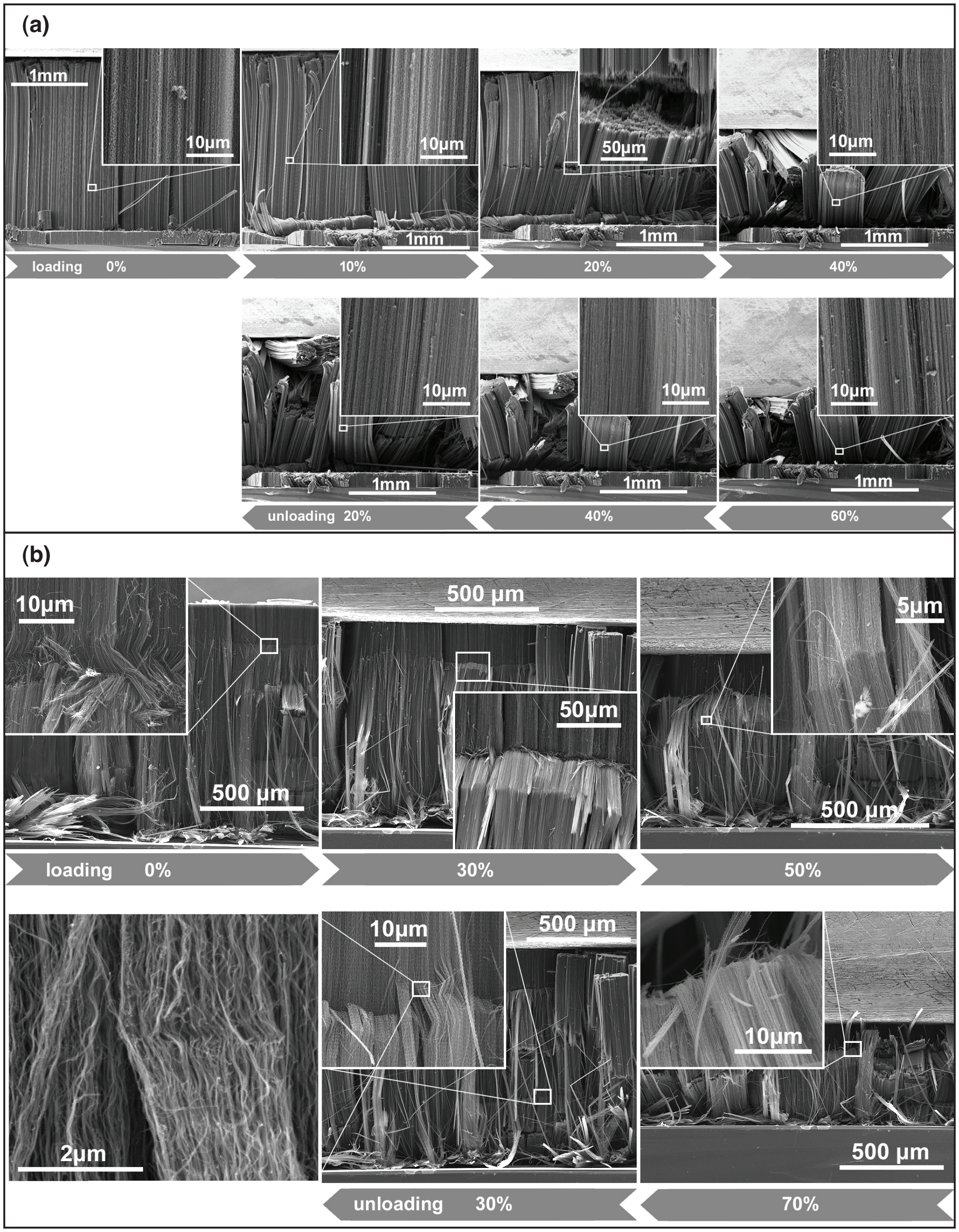

Figure 4.4. (a) SEM image sequence of a pristine HCNT foam sample under a quasistatic compression cycle up to 60% compression. Structural buckle formation at the bottom low-density region and the bundle fracturing upon further compression are observable in the images. **(b)** SEM image sequence of a pre-compressed HCNT foam sample under a

quasistatic compression cycle up to 70% compression. Structural buckle formation and the buckle induced microstructural changes are observable in the images. The bulk sample shows significant recovery upon unloading with traces of the deformation history in the micro-scale. These SEM images were obtained as follows: first an HCNT foam sample was compressed on the *Instron* compression testing system up to 80% strain; then the externally fractured edges of the recovered sample was removed to view the inside of the sample; finally, the sample was subjected to a static loading-unloading cycle in a custom-made vice to perform SEM at different compressive strains.

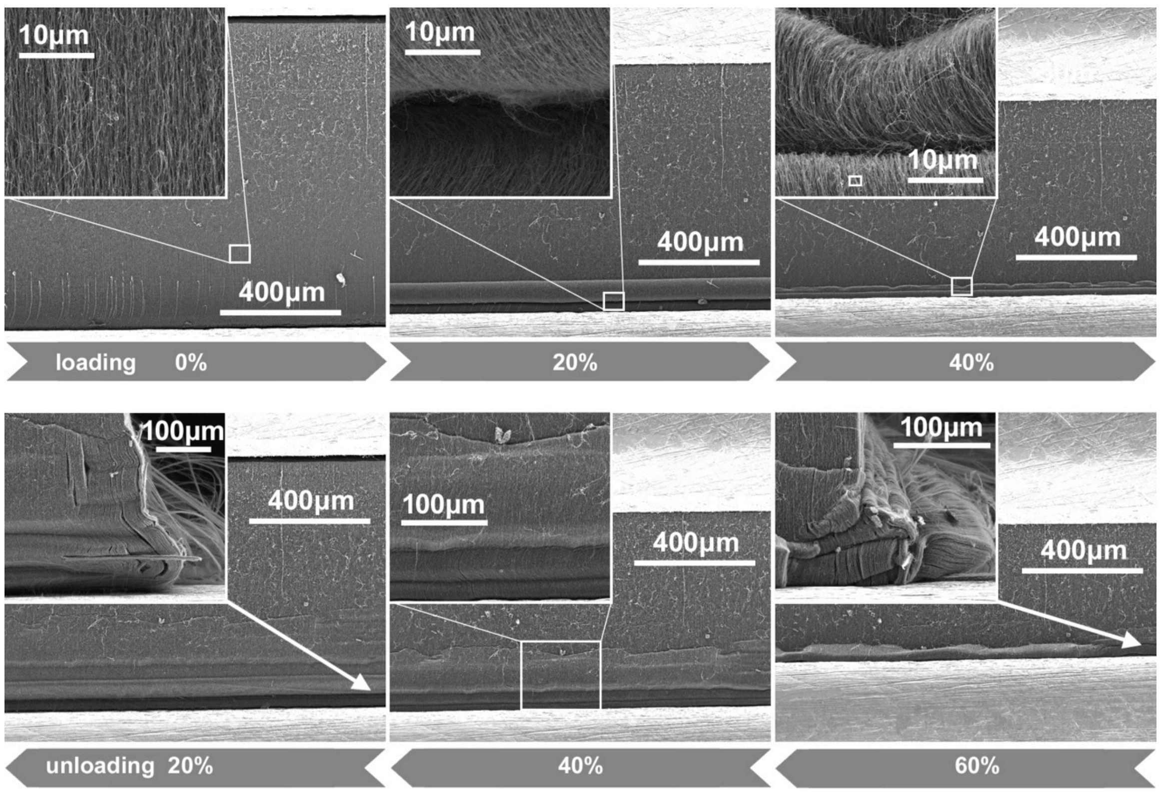

Figure 4.5. SEM image sequence of a pristine VACNT foam subjected to a quasistatic compression cycle up to 60% strain. The collective buckle formation and sequential progression of the buckles from the bottom soft region towards upper stiffer region can be seen on the images. The sample shows a significant recovery upon unloading. The SEM at different compressive strains was performed while statically compressing the sample in a custom-made vice.

The presence of quasistatic compression-induced strain localization at arbitrary regions along the height of the sample also implies that the influence of the intrinsic density gradient along the thickness of the foam is less significant compared to the influence of the nanoscale defects described above. A closer look at the stress-strain response of the HCNT foams (Figure 4.3 (e)) shows that the transition regions, from preconditioned to pristine loading paths, are smooth—in contrast to the sharp transitions observed in VACNT foams [62]. This suggests that the strain localization in HCNT foams is not confined to a narrow region of the foam's thickness (as in the case of the well-defined periodic sequential buckles forming in VACNT foams) [37,123], but the deformation extends to several adjacent pitches of the individual HCNTs. This is also evident from SEM images obtained on a compressed sample where several adjacent pitches of the individual helical coils are distorted by bending, buckling and twisting (Figure 4.3 (g)). An SEM image sequence for a VACNT foam sample subjected to a quasistatic loading-unloading cycle is given in Figure 4.5. Due to these drastically different deformation mechanisms, the loading path of the stress-strain diagram does not show any saw-tooth plateau region with local stress rises and drops, which is a typical characteristic of the formation of localized periodic sequential instabilities [37,123].

4.3.3 Dynamic response of HCNT foams

To study the dynamic response of HCNT foams, we performed controlled impact experiments using a flat plunge striker [169]. In the dynamic regime, the HCNT foams exhibit a nonlinear stress-strain response with hysteresis loop (Figures 4.6 (a) and (b)), similar to the response observed in quasistatic regime. Figure 4.6 (a) shows the stress-strain response of an HCNT foam that was impacted repeatedly at increasing velocities. The stress-strain diagrams show the presence of preconditioning effects and strain localization. Similar to the quasistatic response, the preconditioned, loading path returns to the pristine loading path as soon as the previous maximum strain is exceeded. In addition to confirming the strain localization in dynamics, this observation suggests that the dynamic loading response is rate-independent. We further verified the rate-independency of the loading response of HCNT foams by testing different HCNT foams at controlled impact velocities, between 1 m s^{-1} and 6 m s^{-1} (Figure 4.6 (b)). The stress-strain diagrams followed similar loading paths for the samples tested at increasing velocities (Figure 4.6 (b)). The dynamic unloading modulus increases with increasing impact velocities, due to the fact that the samples reach higher maximum strains (and densification) with increasing impact velocities (Figure 4.6 (c)). The dynamic unloading moduli measured were nearly half of the quasistatic unloading moduli (at 0.8 strain), suggesting that HCNT foams are more compliant in a dynamic than a quasistatic state. This dynamic effect may have arisen from the faster, spring-like pushback response of HCNT foams during striker impacts.

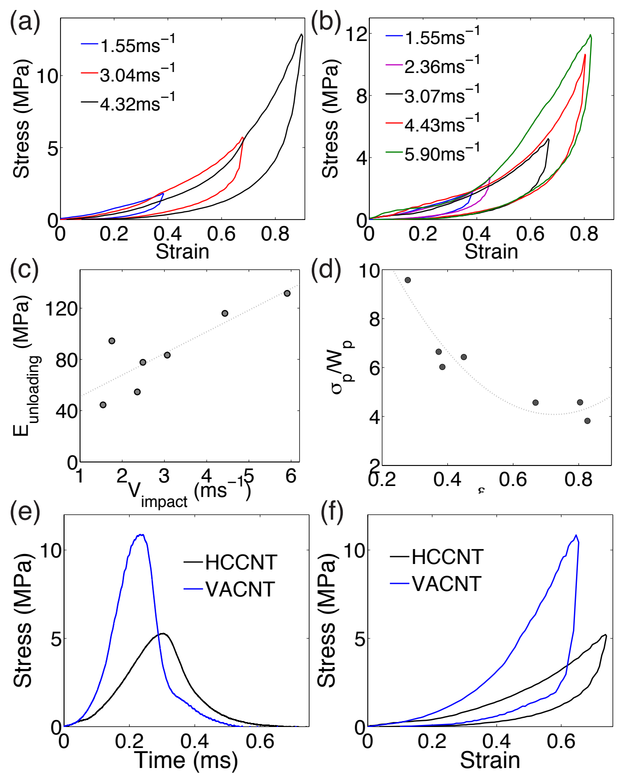

Figure 4.6. Impact response of the HCNT foams. **(a)** Response of an HCNT foam subjected to repeated impacts at increasing velocities. **(b)** Dynamic stress-strain response of different HCNT foams at increasing impact velocities. **(c)** Dynamic unloading modulus with the impact velocity. **(d)** Dynamic cushion factor (peak stress divided by energy absorbed up to peak stress) with maximum strain reached on impacts. **(e)** Characteristic stress-time history of an HCNT foam compared to a VACNT foam with similar density; both samples were impacted at similar velocities (~3 m s^{-1}). **(f)** Dynamic

stress-strain response of the HCNT and VACNT foams.

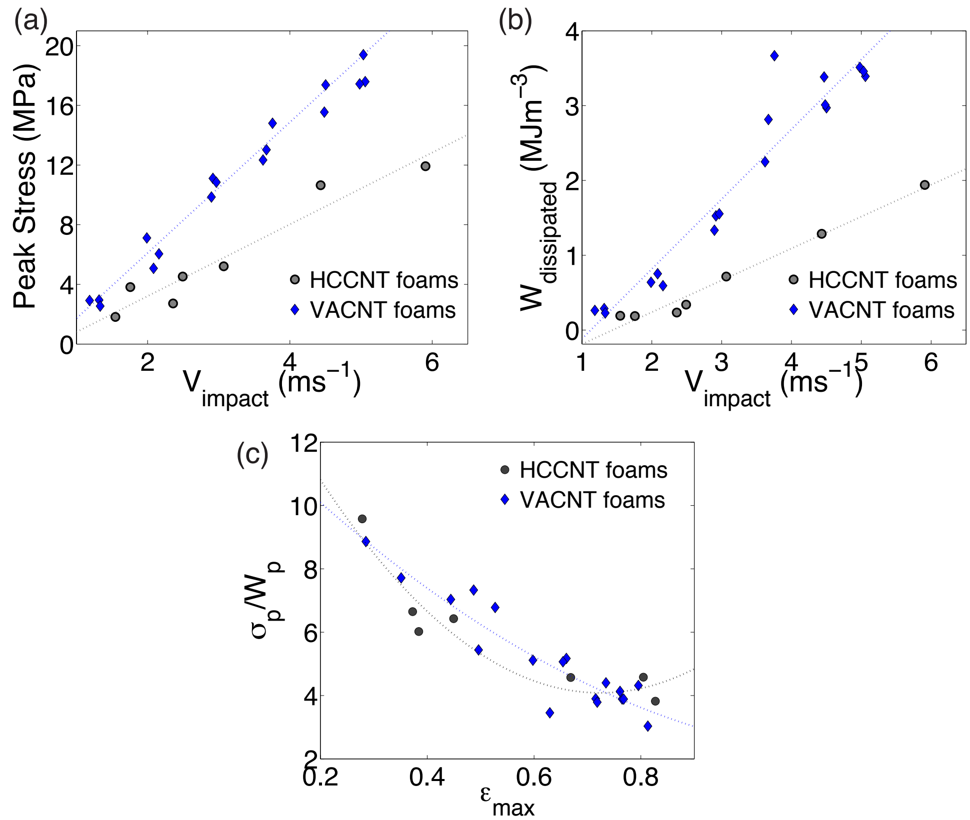

Figure 4.7. Comparison between dynamic responses of HCNT foams and VACNT foams. **(a)** Peak stress with impact velocity; HCCNT foams exhibit lower peak stress compared to VACNT foams. **(b)** Hysteretic energy dissipation with impact velocity; VACNT foams dissipate higher energy compared to HCCNT foams. **(c)** Dynamic cushion factor with maximum strain reached on impact; HCNT foams and VACNT foams exhibit similar cushioning ability.

To show the cushioning ability of the HCNT foams, we plot the variation of dynamic cushion factor with the maximum strain reached on impact (Figure 4.6 (d)). The dynamic cushion factor is calculated by dividing the peak stress by the energy absorbed by the sample up to the peak stress. A decrease in peak stress and/or an increase in energy absorption reduce the dynamic cushion factor—and are beneficial for impact-protective applications. The dynamic cushion factors of HCNT foams are comparable to those of VACNT foams of similar densities [166]. Figure 4.7 (c) presents a comparison of the dynamic cushion factor obtained in HCNT foams and VACNT foams with comparable densities. Even though the HCNT foams and VACNT foams exhibit similar dynamic cushion factors, it should be noted that the VACNT foams exhibit higher hysteretic energy dissipation (Figure 4.7 (b)), by reaching higher peak stresses for a given impact velocity. HCNT foams, however, perform better in damping the impact force amplitude (Figure 4.7 (a)). This improved damping is also evident from the comparison of characteristic dynamic stress-time curves (Figure 4.6 (e)), and dynamic stress-strain diagrams (Figure 4.6 (f)), for HCNT foams and VACNT foams impacted at similar velocities (2.99±0.07 ms^{-1}). At this impact velocity the HCNT foams show ~53% improved impact stress damping over the VACNT foams. The HCNT foams deform more at moderate stress levels and the stress profiles span over a longer duration compared to VACNT foams. This demonstrates that HCNT foams mitigate impacts more effectively by reducing the amplitude of the transmitted stress. The specific damping capacity—i.e., the hysteretic energy dissipated normalized by the energy absorbed up to the peak stress—of all the HCNT foams tested in this study is on average ~0.56±0.07. This implies that ~45% of the energy absorbed by the HCNT foams is stored elastically and released as the striker gains rebound velocity. VACNT foams with similar densities stored only 28% of the absorbed energy as elastic energy and dissipated the rest (72%) [166] (Figure 4.7 (b)). This comparison demonstrates the fundamental role of the helically coiled microstructure of the HCNT foams as opposed to the aligned straight CNTs in the VACNT foams.

We characterized the fundamental deformation mechanisms during impact using *in-situ* high-speed microscopy [169]. Characteristic deformation micrographs and the corresponding dynamic stress-strain diagram of an HCNT foam impacted at 4.43 m s^{-1} are shown in Figure 4.8 and in Supplementary Video 4.1. As evident from the image sequence 1-4, when the HCNT foam is impacted it undergoes an initial compression without an apparent deformation localization. Crushing initiates in the low-density region of the sample adjacent to the substrate and progresses as the striker compresses the foam. After reaching the peak stress at maximum compression (image 4 of Figure 4.8), the sample unloads rapidly by pushing the striker back and eventually detaches from the force sensor. This deformation mechanism in dynamic loading is significantly different from the previously described quasistatic deformation mechanisms of HCNT foams: the intrinsic density gradient governs the progressive deformation whereas, in the quasistatic compression, the presence of nanoscale defects dominates the strain localization at arbitrarily weak locations. The HCNT foam shown in Figure 4.8 recovered 90% of its compressive strain upon unloading. All HCNT foams tested in impact showed a significant recovery, on average 91.5±6.3%. At high impact velocities (>4 m s^{-1}), the edges of the samples underwent brittle fracture (image 5 of Figure 4.8) and several pieces of fractured debris could be seen flying off the sample on the high-speed video during detachment (Supplementary Video 4.1).

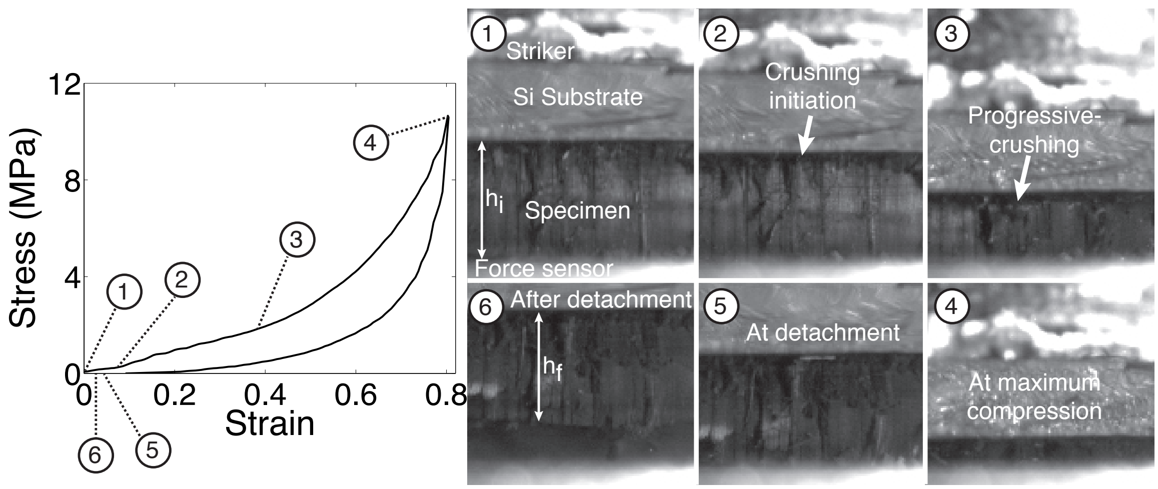

Figure 4.8. Deformation micrographs of an HCNT foam impacted by a striker at 4.43 m s^{-1}. In the dynamic stress-strain diagram (left figure) the circled numbers identify selected snapshots from the high-speed microscopic optical image sequence, which show the foam's deformation.

4.4 Conclusions

In conclusion, we studied the mechanical response of HCNT foams subjected to quasistatic and dynamic loadings. In the quasistatic regime, HCNT foams are characterized by strain localizations and structural buckles occurring at arbitrary weak sections through thickness. Micro-scale brittle fracture of HCNT bundles is also common, although the bulk samples significantly recover their deformation. We supported the mechanical tests with SEM/TEM analysis and identified the microstructure contribution to the observed deformation mechanisms. In the dynamic regime, the HCNT foams follow different deformation mechanisms, characterized by the presence of rate-effects and progressive crushing. We compare the response of HCNT foams to VACNT foams and identify significantly different micro-scale deformation mechanisms in HCNT foams. HCNT foams exhibit better impact absorption characteristics compared to VACNT foams. These observations suggest that the HCNT foams can serve as excellent candidates in developing improved protective materials for energy dissipation and impact absorption.